Biogeosciences
Discussions

Temporal dynamics of surface ocean carbonate chemistry in response to natural and simulated upwelling events during the 2017 coastal El Niño near Callao, Peru

Shao-Min Chen[1, 2], Ulf Riebesell[1], Kai G. Schulz[3], Elisabeth von der Esch[1], Eric P. Achterberg[1], and Lennart T. Bach[4]

[1]GEOMAR Helmholtz Centre for Ocean Research Kiel, Kiel, Germany
[2]Department of Earth and Environmental Sciences, Dalhousie University, Halifax, Canada
[3]Centre for Coastal Biogeochemistry, School of Environment, Science and Engineering, Southern Cross University, Lismore, Australia
[4]Institute for Marine and Antarctic Studies, University of Tasmania, Tasmania, Australia

Correspondence to: Shao-Min Chen (shaomin.chen@dal.ca)

Biogeosciences Open Access

Discussions

EGU

13 **Abstract.** Oxygen minimum zones (OMZs) are characterized by enhanced carbon dioxide (CO_2) levels and low pH and are

14 being further acidified by uptake of anthropogenic atmospheric CO_2. With ongoing intensification and expansion of OMZs

15 due to global warming, carbonate chemistry conditions may become more variable and extreme, particularly in the Eastern

16 Boundary Upwelling Systems. In austral summer (Feb-Apr) 2017, a large-scale mesocosm experiment was conducted in the

17 coastal upwelling area off Callao (Peru) to investigate the impacts of on-going ocean deoxygenation on biogeochemical

18 processes, coinciding with a rare coastal El Niño event. Here we report on the temporal dynamics of carbonate chemistry in

19 the mesocosms and surrounding Pacific waters over a continuous period of 50 days with high temporal resolution observations

20 (every 2nd day). The mesocosm experiment simulated an upwelling event in the mesocosms by addition of nitrogen (N)-

21 deficient and CO_2-enriched OMZ water. Surface water in the mesocosms was acidified by the OMZ water addition, with pH_T

22 lowered by 0.1-0.2 and pCO_2 elevated to above 900 µatm. Thereafter, surface pCO_2 quickly dropped to near or below the

23 atmospheric level (405.22 µatm in 2017, NOAA/GML) mainly due to enhanced phytoplankton production with rapid CO_2

24 consumption. Further observations revealed that the dominance of dinoflagellate *Akashiwo sanguinea* and contamination of

25 bird excrements played important roles in the dynamics of carbonate chemistry in the mesocosms. Compared to the simulated

26 upwelling, natural upwelling events in the surrounding Pacific waters occurred more frequently with sea-to-air CO_2 fluxes of

27 4.2-14.0 mmol C m^{-2} d^{-1}. The positive CO_2 fluxes indicated our site was a local CO_2 source during our study, which may have

28 been impacted by the coastal El Niño. However, our observations of DIC drawdown in the mesocosms suggests that CO_2

29 fluxes to the atmosphere can be largely dampened by biological processes. Overall, our study characterized carbonate

30 chemistry in near-shore Pacific waters that are rarely sampled in such temporal resolution and hence provided unique insights

31 into the CO_2 dynamics during a rare coastal El Niño event.

32 **1 Introduction**

33 One of the most extensive oxygen minimum zones (OMZs) in the global ocean can be found off central/northern Peru (4 - 16°

34 S, Chavez and Messié, 2009). High biological productivity is stimulated by permanent upwelling of cold, nutrient-rich water

35 to the surface supporting a remarkable fish production off Peru (Chavez et al., 2008; Montecino and Lange, 2009; Albert et

36 al., 2010). The high primary production also leads to enhanced remineralization of sinking organic matter in subsurface waters

37 which depletes dissolved oxygen (O_2) and creates an intense and shallow OMZ (Chavez et al., 2008). The depletion of O_2 in

38 OMZs plays an important role in the global nitrogen (N) cycle, accounting for 20 - 40% N loss in the ocean (Lam et al., 2009;

39 Paulmier and Ruiz-Pino, 2009). Denitrification and anammox processes that occur in O_2 depleted waters remove N from the

40 ocean and produce an N deficit and hence phosphorus (P) excess with respect to the Redfield ratio (C:N:P = 106:16:1) in the

41 water column (Redfield, 1963; Deutsch et al., 2001; Deutsch et al., 2007; Hamersley et al., 2007; Galán et al., 2009; Lam et

42 al., 2009). Upwelling of this N-deficient water has been found to control the surface-water nutrient stoichiometry and thus

43 influence phytoplankton growth and community compositions (Franz et al., 2012; Hauss et al., 2012).

44 Apart from being N-deficient, the OMZ waters are also characterized by enhanced carbon dioxide (CO_2) concentrations and

45 low pH from respiratory processes and are further acidified by uptake of anthropogenic atmospheric CO_2 (Feely et al., 2008;

46 Friederich et al., 2008; Paulmier et al., 2008; Paulmier et al., 2011). Accordingly, surface water carbonate chemistry is

47 influenced by upwelling of CO_2-enriched OMZ water (Van Geen et al., 2000; Capone and Hutchins, 2013). The upwelled

48 CO_2-enriched OMZ water can give rise to surface CO_2 levels >1,000 µatm, pH values as low as 7.6, and under-saturation for

49 the calcium carbonate mineral aragonite (Feely et al., 2008; Hauri et al., 2009). As a result, there is a significant flux of CO_2

50 from the ocean to the atmosphere off Peru, which is further facilitated by surface ocean warming, making the Peruvian

51 upwelling region a year-round CO_2 source to the atmosphere (Friederich et al., 2008). In contrast, rapid utilization of upwelled

52 CO_2 and nutrients by phytoplankton can occasionally deplete surface CO_2 below atmospheric equilibrium and dampen the CO_2

53 outgassing (Van Geen et al., 2000; Friederich et al., 2008; Loucaides et al., 2012). The enhanced primary production in turn

54 contributes to increasing export of organic matter, enhanced bacterial respiration, O_2 consumption and CO_2 production at

55 depth. Such a positive feedback may determine the intensity of the underlying OMZ and promote carbon (C) preservation in

56 marine sediments (Dale et al., 2015).

57 In response to reduced O_2 solubility and enhanced stratification induced by global warming, OMZs have been intensifying and

58 expanding over the past decades (Stramma et al., 2008; Fuenzalida et al., 2009; Stramma et al., 2010). Based on regional

59 observations and model projections, a decline in dissolved O_2 concentrations has been reported for most regions of the global

60 ocean (Matear et al., 2000; Matear and Hirst, 2003; Whitney et al., 2007; Stramma et al., 2008; Keeling et al., 2009; Bopp et

61 al., 2013; Schmidtko et al., 2017; Oschlies et al., 2018). The vertical expansion of OMZs represents shoaling of CO_2-enriched

62 seawater, which has become further enriched by oceanic uptake of anthropogenic CO_2 (Doney et al., 2012; Gilly et al., 2013;

63 Schulz et al., 2019). Since biogeochemical processes in OMZs are directly linked to the C cycle and control surface nutrient

64 stoichiometry, with on-going ocean warming and acidification, the deoxygenation may have cascading effects on plankton

65 productivity and composition, C uptake, and food web functioning (Keeling et al., 2009; Gruber, 2011; Doney et al., 2012;

66 Gilly et al., 2013; Levin and Breitburg, 2015). Therefore, it is important to monitor the changes in CO_2 when investigating the

67 effects of deoxygenation on marine ecosystems.

68 To investigate the potential impacts of upwelling on pelagic biogeochemistry and natural plankton communities in the Peruvian

69 OMZ, a large-scale *in situ* mesocosm study was carried out in the coastal upwelling area off Peru. An upwelling event was

70 simulated in the mesocosms by addition of OMZ waters collected from two different locations where the OMZ was considered

71 to contain different nutrient concentrations and N:P ratios. The ecological and biogeochemical responses in the mesocosms

72 were monitored and compared with those influenced by natural upwelling events in the ambient coastal water surrounding the

73 mesocosms. As part of this collaborative research project, questions specific to the present paper were: (1) How does surface

74 water carbonate chemistry respond to an upwelling event?; and (2) How does upwelled OMZ water with different chemical

75 signatures modulate surface water carbonate chemistry? The current study will mainly focus on the temporal changes in surface

76 water carbonate chemistry within the individual mesocosms, including observations made in the ambient Pacific water and a

77 local estimate of air-sea CO_2 exchange, together with the influence by a rare coastal El Nino event (Garreaud, 2018). This

78 provides first insights into how inorganic C cycling links to chemical signatures of OMZ waters in a natural plankton

79 community and its implications for ongoing environmental changes.

80 **2 Material and methods**

81 **2.1 Study site**

82 The experiment was conducted in the framework of the Collaborative Research Center 754 "Climate-Biogeochemistry

83 Interactions in the Tropical Ocean" (www.sfb754.de/en) and in collaboration with the Instituto del Mar del Peru (IMARPE)

84 in Callao, Peru (Fig. 1a). The coastal area off Callao lies within the Humboldt Current System and is influenced by wind-

85 induced coastal upwelling (Bakun and Weeks, 2008).

86 **2.2 Mesocosm setup**

87 Eight "Kiel Off-Shore Mesocosms for Future Ocean Simulations" (KOSMOS) units (M1-M8), extending 19 m below the sea

88 surface, were deployed by the research vessel *Buque Armada Peruana (BAP) Morales* and moored at 12.06° S, 77.23° W in

89   the coastal upwelling area off Callao, Peru (Fig. 1a) on February 23rd, 2017 (late austral summer). The technical design of

90   these sea-going mesocosms is described by Riebesell et al. (2013). For a more detailed description of the mesocosm

91   deployment and maintenance in this study, please refer to Bach et al. (2020a).

92   The mesocosm bags were filled with surrounding seawater through the upper and lower openings. Both openings were covered

93   by screens with a mesh size of 3 mm to avoid enclosing larger organisms such as fish. The mesocosm bags were left open

94   below the water surface for two days, allowing free exchange with surrounding coastal water. On February 25th, mesocosm

95   bags were closed with the screens removed, tops pulled above the sea surface and bottoms sealed with 2-m long conical

96   sediment traps (Fig. 1b). The experiment started with the closure of the mesocosms (day 0) and lasted for 50 days. Each

97   mesocosm bag enclosed a seawater volume of ~54 m^3. After the bags were closed, daily or every-2nd-day sampling was

98   performed to monitor the initial conditions of the enclosed water before simulating an upwelling event on day 11 and 12 (see

99   Sect. 2.4 for details).
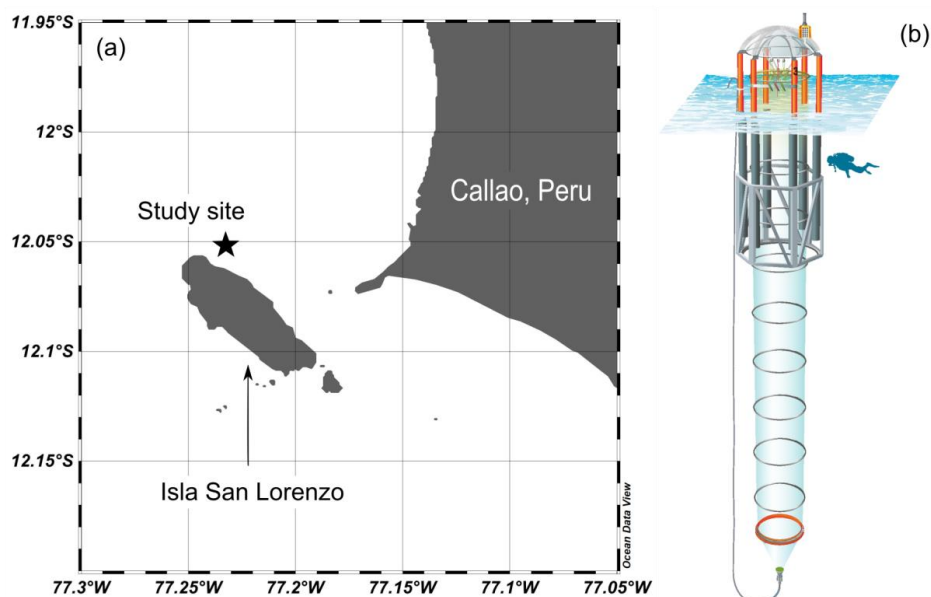
100
101 **Figure 1 The study site of the mesocosm experiment (a) created and modified using Ocean Data View (Schlitzer, Reiner, Ocean**
102 **Data View, odv.awi.de, 2021) and a schematic illustration of a KOSMOS mesocosm unit (b). We acknowledge reprint permission**
103 **from the AGU as parts of this drawing was used for a publication by Bach et al. (2016). The star symbol marks the approximate**
104 **location of mesocosm deployment.**

105 **2.3 Simulated upwelling and salt addition**

106 To simulate an upwelling event in the mesocosms, OMZ-influenced waters were collected from the nearby coastal area and

107 added to the mesocosms. Two OMZ water masses were collected at Station 1 (12° 01.70' S, 77° 13.41' W) at a depth of ~30

108 m and at Station 3 (12° 02.41' S, 77° 22.50' W) at a depth of ~70 m respectively using a deep-water collection system as

109 described by Taucher et al. (2017). These two water masses were sampled for chemical and biological variables as the

110 mesocosms (see Sect. 2.4). The OMZ water collected from Station 3 had a dissolved inorganic nitrogen (DIN) concentration

111 of 4.3 μmol L^{-1} (denoted as "Low DIN" in this paper) and was added to M2, M3, M6 and M7. The OMZ water from Station 1

112 had a DIN of 0.3 μmol L^{-1} (denoted as "Very low DIN" in this paper) and was added to M1, M4, M5 and M8. Before OMZ

113 water addition, approximately 9 m^3 of seawater were removed from 11-12 m of each mesocosm on March 5th (day 8). During

114 the night of March 8th (day 11), ~10 m^3 of OMZ water were added to 14-17 m of each mesocosm. On March 9th (day 12), ~10

115 m^3 of seawater were removed from 8-9 m followed by an addition of ~12 m^3 OMZ water to 0-9 m of each mesocosm.

4

116   To maintain a low-O_2 bottom layer in the mesocosms and avoid convective mixing induced by heat exchange with the

117   surrounding Pacific, 69 L of a concentrated sodium chloride (NaCl) brine solution were added to the bottom of each mesocosm

118   (10-17 m) on day 13, which increased the bottom salinity by ~0.7 units. Since then, turbulent mixing induced by sampling

119   activities continuously interrupted the artificial halocline. Hence, on day 33, 46 L of the NaCl brine solution were added again

120   to the bottom of each mesocosm (12.5-17 m), which increased the bottom salinity by ~0.5 units. At the end of the experiment

121   after the last sampling (day 50), 52 kg of NaCl brine was added again to each mesocosm to calculate the enclosed seawater

122   volume from a measured salinity change by ~0.2 units (see Czerny et al., 2013 and Schulz et al., 2013 for details). The average

123   final volume for each mesocosm bag was calculated at ~54 m^3. With known sampling volumes and deep-water addition

124   volumes during the experiment, the enclosed volumes of each mesocosm on each sampling day could be calculated. The NaCl

125   solution for the halocline establishments had been prepared in Germany by dissolving 300 kg of food industry grade NaCl

126   (free of anti-caking agents) in 1000 L deionized water (Milli-Q, Millipore) and purified with ion exchange resin (LewawitTM

127   MonoPlus TP260®, Lanxess, Germany) to minimize potential contaminations with trace metals (Czerny et al., 2013). The

128   NaCl solution for the volume determination was produced on site using locally purchased table salt. For a more detailed

129   description of OMZ water and salt additions, please refer to Bach et al. (2020a).

130   **2.4 Sampling procedures and CTD operations**

131   Sampling was carried out in the morning (7 a.m.-11 a.m. local time) daily or every 2nd day throughout the entire experimental

132   period. Depth-integrated samples were taken from the surface (0-10 m for day 3-28) and bottom layer (10-17 m for day 3-28)

133   of the mesocosms and the surrounding coastal water (named "Pacific") using a 5-L integrating water sampler (IWS, HYDRO-

134   BIOS, Kiel). Due to the deepening of the oxycline as observed from the CTD profiles, the sampling depth for the surface was

135   adjusted to 0-12.5 m while that for the bottom was changed to 12.5-17 m from day 29 until the end of the experiment (day 50).

136   For gas-sensitive variables such as pH and dissolved inorganic carbon (DIC), 1.5 L of seawater from each integrated depth in

137   each mesocosm were taken directly from the fully-filled 5-L integrating water sampler. Clean polypropylene sampling bottles

138   (rinsed with deionized water in the laboratory; Milli-Q, Millipore) were pre-rinsed with sample water immediately prior to

139   sampling. Bottles were filled from bottom to top using pre-rinsed Tygon tubing with overflow of at least one sampling bottle

140   volume (1.5 L) to minimize the impact of CO_2 air-water gas exchange. Nutrient samples were collected into 250 ml

141   polypropylene bottles using pre-rinsed Tygon tubing (see Bach et al., 2020a for details). Sample containers were stored in cool

142   boxes for ~3 hours, protected from sunlight and heat before being transported to the shore. Once in the lab, sample water was

143   sterile-filtered by gentle pressure using syringe filters (0.2 μm pore size), Tygon tubing and a peristaltic pump to remove

144   particles that may cause changes to seawater carbonate chemistry (Bockmon and Dickson, 2014). For DIC measurements, the

145   water was filtered from the bottom of the 1.5-L sample bottle into 100-ml glass-stoppered bottles (DURAN) with an overflow

146   of at least 100 ml to minimize contact with air. Once the glass bottle was filled with sufficient overflow, it was immediately

147   sealed without headspace using a round glass stopper. This procedure was repeated to collect a second bottle (100 ml) of

148   filtered water for pH measurements. The leftover seawater was directly filtered into a 500 ml polypropylene bottle for total

149   alkalinity (TA) measurements (non-gas-sensitive). Filtered DIC and pH samples were stored at 4 ℃ in the dark and TA samples

150   were at room temperature in the dark until further analysis. Samples were analysed for DIC and pH on the same day of

151   sampling, while TA was determined overnight (see Sect. 2.5 for analytical procedures).

152   CTD casts were performed with a multiparameter logging probe (CTD60M, Sea and Sun Technology) in the mesocosms and

153   Pacific on every sampling day. From the CTD casts, profiles of salinity, temperature, pH, dissolved O_2, chlorophyll *a* (chl *a*)

154   and photosynthetically active radiation were obtained (see Schulz and Riebesell, 2013 and Bach et al., 2020a for details).

2.5 Carbonate chemistry and nutrient measurements

Total alkalinity was determined at room temperature (22-32℃) by a two-stage open-cell potentiometric titration using a Metrohm 862 Compact Titrosampler, Aquatrode Plus (Pt1000) and a 907 Titrando unit in the IMARPE laboratory following Dickson et al. (2003). The acid titrant was prepared by preparing a 0.05 mol kg^{-1} hydrochloric acid (HCl) solution with an ionic strength of ca. 0.7 mol kg^{-1} (adjusted by NaCl). Approximately 50-grams of sample water from each sample was weighed into the titration cell with the exact weight recorded (precision: 0.0001 g). After the two-stage titration, the titration data between a pH of ~3.5 and 3 was fitted to a modified non-linear Gran approach described in Dickson et al. (2007) using MATLAB (The MathWorks). The results were calibrated against certified reference materials (CRMs) batch 142 (Dickson, 2010) measured on each measurement day. In this paper, measured TA values refer to the measured values that have been calibrated against the CRM.

Seawater pH_T (total scale) was determined spectrophotometrically by measuring the absorbance ratios after adding the indicator dye m-cresol purple (mCP) as described in Carter, et al. (2013). Before measurements, samples were acclimated to 25.0°C in a thermostatted bath. The absorbance of samples with mCP was determined on a Varian-Cary 100 double-beam spectrophotometer (Varian), scanning between 780 and 380 nm at 1-nm resolution. During the spectrophotometric measurement, the temperature of the sample was maintained at 25.0°C by a water-bath connected to the thermostatted 10-cm cuvette. The pH_T values were calculated from the baseline-corrected absorbance ratios and corrected for *in situ* salinity (obtained from CTD casts) and pH change caused by dye addition (using the absorbance at the isosbestic point, i.e. 479 nm) as described in Dickson et al. (2007). To minimize potential CO_2 air-water gas exchange, a syringe pump (Tecan Cavro XLP) was used for sample/dye mixing and cuvette injection (see Schulz et al. 2017 for details). For the dye correction, a batch of sterile filtered seawater of known salinity was prepared. The pH_T was determined once for an addition of 7 ul of dye and once of 25 ul at five pH levels (raised to 7.95 with NaOH and lowered to 7.74, 7.58, 7.49 and 7.36 with HCl stepwise). The pH change resulting from the dye correction addition was calculated from the change in measured absorbance ratio for each pair of dye additions (see Clayton and Byrne, 1993 and Dickson et al., 2007 for details). The dye-corrected pH_T values measured at 25.0°C and atmospheric pressure were then re-calculated for *in situ* temperature and pressure as determined by CTD casts (averaged over 0-10/12.5 m for surface and 10/12.5-17 m for bottom). For carbonate chemistry speciation calculations (see Sect. 2.6), the dye-corrected pH_T values were used as one of the input parameters.

Dissolved inorganic carbon was measured by infrared absorption using a LI-COR LI-7000 on an AIRICA system (MARIANDA, Kiel, see Taucher et al., 2017 and Gafar and Schulz, 2018 for details). The results were calibrated against CRMs batch 142 (Dickson, 2010). Unfortunately, due to a malfunctioning of the AIRICA system, we obtained measured DIC data only up to March 7th (day 10). Therefore, measured TA and pH_T were used for calculations of carbonate system parameters at *in situ* temperature and salinity but we used DIC measurements from day 3-10 for consistency checks of calculated carbonate chemistry parameters. In this paper, measured DIC values refer to the measured values that have been calibrated against the CRM.

Inorganic nutrients were analyzed colorimetrically (NO_3^-, NO_2^-, PO_4^{3-} and $Si(OH)_4$) and fluorimetrically (NH_4^+) using a continuous flow analyzer (QuAAtro AutoAnalyzer with integrated photometers, SEAL Analytical) connected to a fluorescence detector (FP-2020, JASCO). All colorimetric methods were conducted according to Murphy and Riley (1962), Mullin and Riley (1955a, b) and Morris and Riley (1963) and corrected following the refractive index method developed by Coverly et al. (2012). For details of the quality control procedures, see Bach et al. (2020a).

2.6 Carbonate chemistry speciation calculations and propagated uncertainties

193

194   Calculations of carbonate chemistry parameters (*in situ* pH_T, DIC, pCO$_2$, and calcium carbonate saturation state for calcite and

195   aragonite) were performed with the Excel version of CO2SYS (Version 2.1, Pierrot et al., 2006) using K1 and K2 dissociation

196   constants from Mehrbach et al., (1973) which were refitted by Lueker et al. (2000). The dissociation constant for KHSO$_4$ from

197   Dickson (1990) and for total boron from Uppström (1974) were applied in the calculations (see Orr et al., 2015 for details).

198   The observed pH_T and TA as well as inorganic nutrient concentration (phosphate and silicic acid) were used as input CO_2

199   system parameters. *In situ* salinity and temperature were obtained by CTD casts and averaged over surface (0-10 m or 0-12.5

200   m) and bottom (10-17 m or 12.5-17 m) waters for each sampling day. In situ pressure was approximated for surface (5 dbar)

201   and bottom (13.5 or 14.75 dbar) waters. For details of calculation procedures and choices of constants, see Lewis et al. (1998)

202   and Orr et al. (2015).

203   To evaluate the performance of pH_T and TA measurements, quality control procedures were performed. First, standard

204   deviations of pH_T measurements were graphed over time. Measured TA values of a control sample (CRM batch 142, Dickson,

205   2010) were plotted over time, compared to the warning and control limits calculated from their mean and standard deviation

206   (for details please see Dickson et al., 2007) as well as the certified value of the CRM. To compute a range control chart for the

207   evaluation of measurement repeatability, the absolute difference between duplicate measurements of CRMs on each sampling

208   day was calculated and plotted over time, compared to the warning and control limits calculated from their mean and standard

209   deviation (for details see Dickson et al., 2007).

210   We used the R package *seacarb* with a Gaussian approach and an input variable pair (pH_T, TA) to calculate uncertainties for

211   calculated CO_2 system parameters (Orr et al. 2018; Gattuso et al. 2020). The contribution of input uncertainties in nutrient

212   concentrations and *in situ* salinity and temperature to the uncertainties in the CO2SYS-based calculations are often small (<

213   0.1%; Orr et al. 2018) so they were not considered in our propagation. The input uncertainties of pH_T and TA were estimated

214   based on our measurements (Table 1). Standard uncertainties include random and systematic errors. For TA, systematic errors

215   were removed by calibrating the measured results using CRMs (see Sect. 2.5). Hence, the random error of TA, estimated by

216   the averaged standard deviation of all the CRM measurements (4.4 µmol kg^{-1}; n = 62), was used as the standard uncertainty.

217   For pH_T, an uncertainty of 0.01 was used as the standard uncertainty. Due to the unavailability of CRMs that correct for

218   systematic error in pH measurements, the standard deviations of repeated measurements (0.0012; n = 377) only accounted for

219   the random components of standard uncertainties (Orr et al. 2018). Therefore, we used 0.01 in our uncertainty propagation as

220   an approximation of the total standard uncertainty for pH_T, which has been used in previous assessments (Orr et al. 2018).

221   **Table 1: Standard uncertainties of pH_T and TA estimated based on our measurements are denoted by u(pHT) and u(TA). Based**
222   **on u(pH$_T$) and u(TA), propagated uncertainties were estimated for each data point in R and averaged for each reported variable**
223   **(µ), with Standard deviation (σ), minimum (min) and maximum (max) values presented. The relative percentage (%) of**
224   **propagated standard uncertainties were calculated by dividing the propagated uncertainty by the corresponding data point and**
225   **averaged for each reported variable (µ), with σ, min and max values presented.**

u(pH$_T$)	u(TA)		ΔpCO$_2$		ΔDIC		$\Delta\Omega_{Ar}$		$\Delta\Omega_{Ca}$	
	µmol kg^{-1}		µatm	%	µmol kg^{-1}	%		%		%
0.01	4.4	µ	35.94	3.8	6.63	0.3	0.08	5.1	0.13	5.1
		σ	12.60	0.3	0.80	0.0	0.03	0.3	0.05	0.3
		min	15.07	3.2	5.88	0.3	0.04	4.4	0.07	4.4
		max	62.84	4.8	8.72	0.4	0.16	5.8	0.24	5.8

226   The air-sea flux of CO_2 (FCO$_2$, mmol C m^{-2} d^{-1}) in the Pacific was determined based on

227    $$FCO_2 = k\, K_0\, \Delta pCO_2$$ (1)

228   where k is the gas transfer velocity parameterized as a function of wind speed, K_0 is the solubility of CO_2 in seawater dependent

229   on *in situ* salinity and temperature (Weiss, 1974), and ΔpCO_2 is the difference between pCO_2 in the surface water and in the

230   atmosphere (Wanninkhof 2014). Wind data were averaged over 2 sampling days for the sampling location from a satellite-

231   derived gridded dataset (GLDAS Model, near surface wind speed, 0.25 x0.25 degrees, 3 hour temporal resolution, 12.375° to

232   11.875°S, 77.375° to 76.875°W), obtained from NASA Giovanni (Rodell et al., 2004; Beaudoing and Rodell, 2020). *In situ*

233   salinity and temperature were obtained from the CTD casts (see Sect. 2.4). Calculated pCO_2 based on (pH_T, TA) and an

234   estimated atmospheric pCO_2 of 405.22 µatm (referenced to year 2017, NOAA/GML) were used in the air-sea flux estimation.

235   **3 Results**

236   **3.1 Responses of surface layer nutrient concentrations**

237   The OMZ-influenced water masses were collected from two locations and added to the mesocosms to simulate an upwelling

238   event (see Sect. 2.3). The two water masses were named "Low DIN" and "Very low DIN" respectively based on their DIN

239   concentrations (Table 2). Both water masses shared similar silicic acid (Si) and phosphate (PO_4^{3-}) concentrations but differed

240   in DIN concentration. The "Low DIN" water had a DIN concentration of 4.3 µmol L^{-1}, 14 times as high as that of the "Very

241   low DIN" water (0.3 µmol L^{-1}; Table 2).

242 **Table 2: Inorganic nutrient concentrations of the two collected deep-water masses. Please note that DIN is the sum of nitrate, nitrite**
243 **and ammonium. P is phosphate. Si is silicic acid. Color codes denote the two water masses and are applied to the mesocosms treated**
244 **with respective water masses in the following figures and tables.**

Water mass	Si (μmol L^{-1})	DIN (μmol L^{-1})	PO$_4^{3-}$ (μmol L^{-1})	N: P ratio (mol: mol)
Low DIN	19.6	4.3	2.5	1.7
Very low DIN	17.4	0.3	2.6	0.1

245 On day 10 before OMZ water addition, the average surface DIN concentration of the two treatment groups were similar (3.4

246 μmol L^{-1}), but lower than that in the Pacific (9.8 μmol L^{-1}; Table 3). Surface layer DIN concentration in the mesocosms ranged

247 between 2.0 and 6.0 μmol L^{-1} before OMZ water addition (Fig. 2a). The addition of OMZ water elevated surface DIN in the

248 "Low DIN" mesocosms to 3.6-6.4 μmol L^{-1} but lowered that in the "Very low DIN" to 0.9-2.0 μmol L^{-1}. The average surface

249 DIN concentration in the "Very low DIN" decreased to 1.6 μmol L^{-1} while the "Low DIN" slightly increased to 4.7 μmol L^{-1}

250 (Table 3), followed by a sharp depletion on day 16 except for M3. M3 received the highest input of DIN (6.4 μmol L^{-1}) and

251 was not depleted until day 24. Despite several small peaks in M3, M4, M5 and M6 ($\leq$ 1.6 μmol L^{-1}), surface DIN concentration

252 in the mesocosms were at around limits of detection (LODs: NH$_4^+$ = 0.063 μmol L^{-1}, NO$_2^-$ = 0.054 μmol L^{-1}, NO$_3^-$ = 0.123

253 μmol L^{-1}) most of the time after depletion. A slight rise could be observed from day 44 towards the last sampling day (day 48).

254 In the Pacific, surface layer DIN concentration was mostly greater than 5 μmol L^{-1} (except on day 16 and 18) and became

255 considerably higher during the second half of the experiment (> 10 μmol L^{-1} for day 26-44; Fig. 2a).

256 **Table 3: DIN concentration (μmol L^{-1}) in the surface layer of each mesocosm (M1-M8) and the average DIN concentration (μmol L^{-1})**
257 **for each treatment ("Low DIN" and "Very Low DIN", n = 4) before (t10) and after deep water addition (t13). The DIN**
258 **concentration in the surface Pacific water is also shown. Color codes and symbols denote the respective mesocosm in the following**
259 **figures.**

	M1	M2	M3	M4	M5	M6	M7	M8	Low DIN	Very Low DIN	Pacific
t10	3.7	2.2	5.0	3.3	3.9	3.4	3.2	2.6	3.4 ± 1.2	3.4 ± 0.5	9.8
t13	1.8	3.6	6.4	2.0	1.6	4.7	4.0	0.9	4.7 ± 1.3	1.6 ± 0.5	9.2
	■	■	●	●	▲	▲	▼	▼			●

260 Surface layer PO$_4^{3-}$ concentrations in the mesocosms initially ranged between 1.1 and 1.5 μmol L^{-1} and were elevated by OMZ

261 water addition to around 1.9 μmol L^{-1} (Fig. 2b). Thereafter, PO$_4^{3-}$ exhibited a slow but steady decline until the end of the study

262 with a slightly higher decrease in "Low DIN" mesocosms (blue symbols; Fig. 2b). Throughout the study, PO$_4^{3-}$ in the

263 mesocosms was never lower than 1.1 μmol L^{-1}. Surface layer PO$_4^{3-}$ in the Pacific was generally higher, fluctuating between

264 1.4 and 2.9 μmol L^{-1}. In the mesocosms, enhanced chl a concentrations were observed at depths shallower than 5 m and below

265 15 m before OMZ water addition (Fig. 2c). Following OMZ water addition, a chl a maximum occurred at ~10 m and persisted

266 until day 40, except for M3 and M4 with a 1-week delayed increase in the former and a lack of bloom in the latter (Fig. 2c).

267 After day 40, chl a concentrations in all mesocosms (except for M4) increased to 12-38 μg L^{-1} with a bloom occurring in 0-10

268 m (Fig. 2c) Throughout the study, a chl a maximum was continuously observed above 10 m in the Pacific (Fig. 2c).
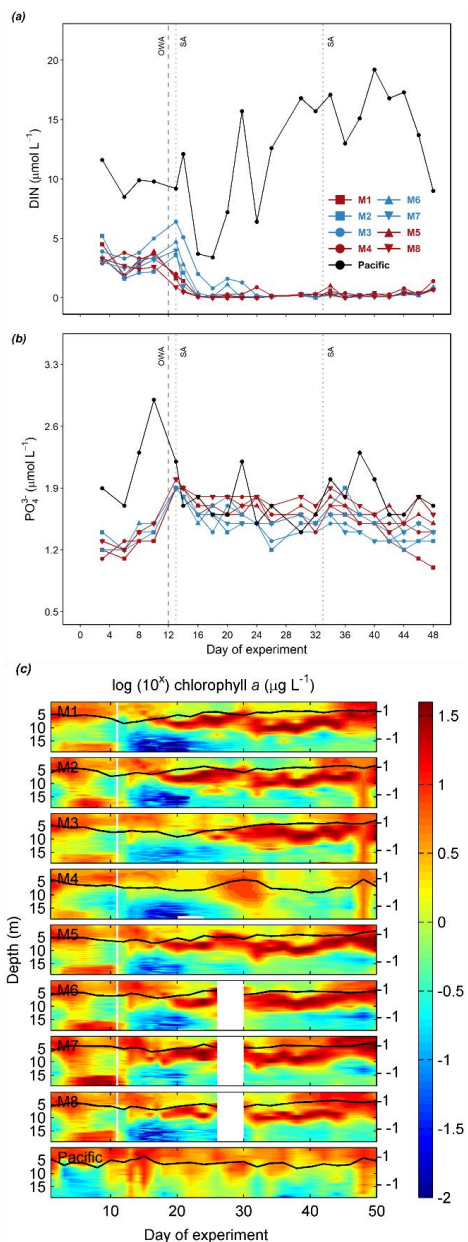
Figure 2 Temporal dynamics of depth-integrated surface DIN concentration (a), PO_4^{3-} concentration(b) and vertical distribution of chl *a* concentration determined by CTD casts (c). The black solid lines on top of the coloured contours represent the average values over the entire water column, with the corresponding additional y-axes on the right. The vertical white lines represent the day when OMZ water was added to the mesocosms. Color codes and symbols denote the respective mesocosm. Abbreviation: OWA, OMZ water addition. SA, salt addition. Dataset is available at https://doi.pangaea.de/10.1594/PANGAEA.923395 (Bach et al., 2020b).

3.2 Temporal dynamics of carbonate chemistry

Before OMZ water addition, surface layer pH_T in the mesocosms ranged between 7.80-7.94 with a slight decline by ~0.1 over time (Fig. 3a). The initial surface layer TA ranged between 2,310 and 2,330 µmol kg^{-1} (Fig. 3b; day 3-12). Surface layer pCO_2 and DIC ranged from 541 to 749 µatm and 2,119 to 2,180 µmol kg^{-1}, respectively (Fig. 3c, d).

279   The two collected OMZ-water masses shared similar carbonate chemistry properties despite the differences in DIN

280   concentrations. In both water masses, pH_T was ~7.48, DIC was ~2,305-2,310 µmol kg^{-1}, TA was ~2,337 µmol kg^{-1}, and pCO_2

281   was between 1,700 and 1,780 µatm (Table 4).

282   **Table 4: The *in situ* pH_T, TA, DIC, pCO_2, Ω_{Ar} and Ω_{Ca} of the two collected OMZ-water masses.**

Water mass	pH_T	TA (µmol kg^{-1})	DIC (µmol kg^{-1})	pCO_2 (µatm)	Ω_{Ar}	Ω_{Ca}
Low DIN	7.49	2336.5	2305.4	1707.5	0.90	1.38
Very low DIN	7.47	2338.2	2312.1	1775.3	0.87	1.34

283   Surface DIC and pCO_2 were elevated from ~2,150 µmol kg^{-1} and ~600 µatm to ~2,200 µmol kg^{-1} and ~900 µatm (except M7)

284   by OMZ water addition, respectively, without distinct differences between the two treatments (Mann-Whitney U-Test, p >

285   0.05; Fig. 3c). Following OMZ water addition, surface pCO_2 in the mesocosms decreased quickly and reached minima at 340-

286   500 µatm (except M3 and M4) on day 24 and 26. These minima corresponded with DIC minima at 2,040-2,110 µmol kg^{-1} and

287   pH_T maxima at 7.9-8.1 (except M3 and M4; Fig. 3c, d). After reaching the minima, surface layer pCO_2 exhibited a steady

288   increase to 410- 680 µatm from day 24 to day 38 and later declined in M3, M5, and M7 while the rest remained relatively

289   stable until day 42 (Fig. 3c). Interestingly, and unlike the other mesocosms, after OMZ water addition, pCO_2 in M3 steadily

290   declined from 928 to 342 µatm until the end of the experiment while that in M4 remained constantly higher than the other

291   mesocosms (> 700 µatm), with a slightly decreasing trend to 645 µatm towards the end of the study (Fig. 3c).

292   In the Pacific, much lower surface pH_T and higher surface pCO_2 and DIC were observed compared to the mesocosms, with an

293   average of 7.7 (7.6-7.8), 1,078 µatm (775 – 1358 µatm) and 2,221 µmol kg^{-1} (2173 – 2269 µmol kg^{-1}; minimum to maximum

294   range in parenthesis; Fig. 3c, d), respectively. TA in the Pacific was initially similar to that in the mesocosms, fluctuating

295   between 2,310 and 2,330 µmol kg^{-1}, and later decreased to ~2,310 µmol kg^{-1} for the rest of the study.

296   Surface waters in the mesocosms and the Pacific were always saturated with respect to calcite and aragonite throughout the

297   entire experimental period, with lower values observed in the Pacific (Fig. 4a, c). Bottom waters in the mesocosms and Pacific

298   were always saturated with respect to calcite during the experiment (Fig. 4b) while bottom waters in the Pacific were

299   undersaturated with respect to aragonite before day 13 (0.88-0.99) and had Ω_{Ar} values slightly above 1.0 for the rest of the

300   study period (Fig. 4d).
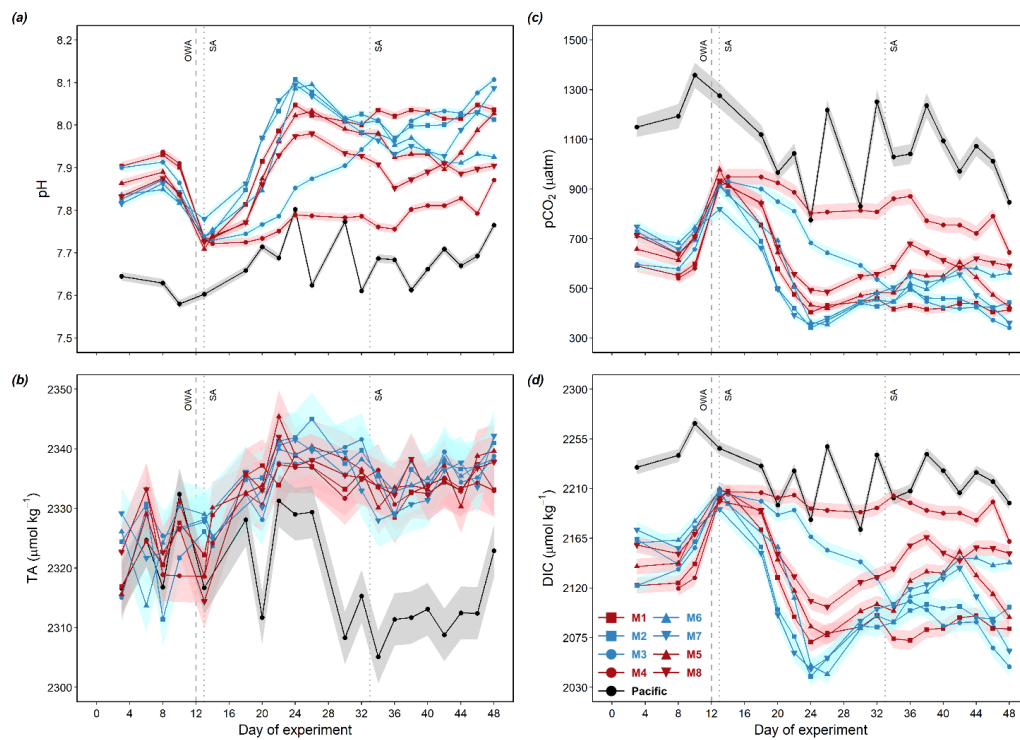
Figure 3 Temporal dynamics of measured depth-integrated surface pH$_T$ (a) and TA (b), and calculated pCO$_2$ (c) and DIC (d). The error ribbons present measurement and propagated standard uncertainties of the calculations, respectively. Color codes and symbols denote the respective mesocosm. Abbreviation: OWA, OMZ water addition. SA, salt addition.
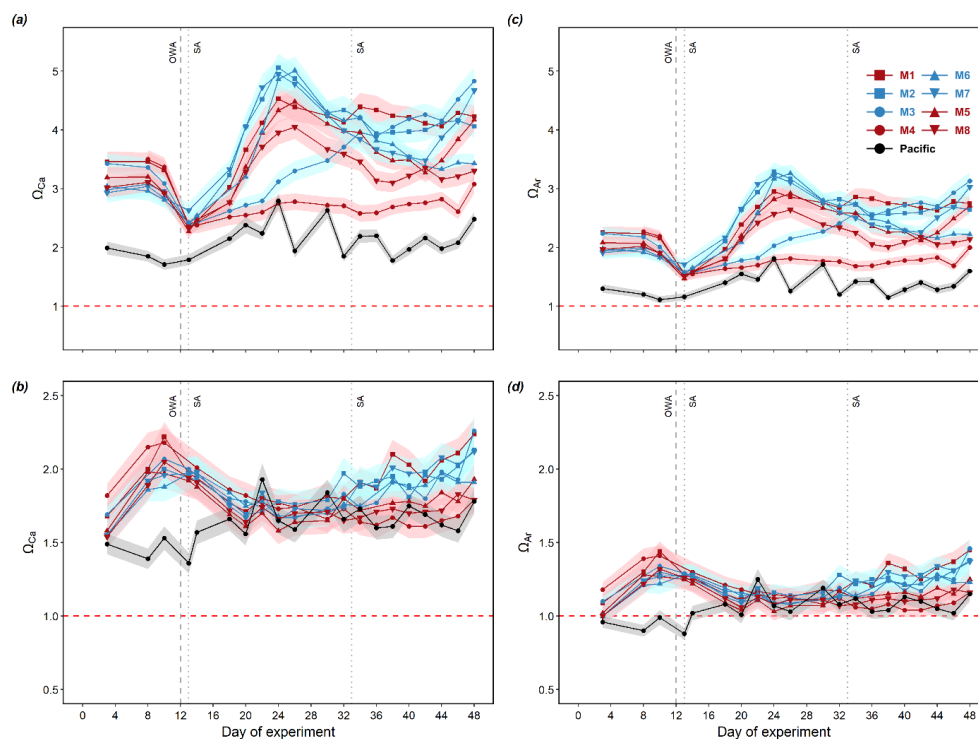
Figure 4 Temporal dynamics of depth-integrated surface calcite saturation state (a), bottom calcite saturation state (b), surface aragonite saturation state (c), and bottom aragonite saturation state (d) in the mesocosms and the surrounding Pacific. The error ribbons present the propagated standard uncertainties of the calculations. When Ω > 1 (above red dashed line), seawater is supersaturated for calcium carbonate. When Ω < 1 (below red dashed line), seawater is under-saturated for calcium carbonate. Color codes and symbols denote the respective mesocosm. Abbreviation: OWA, OMZ water addition. SA, salt addition.

3.3 Air-sea CO_2 fluxes in the Pacific

Positive FCO_2 values indicate CO_2 outgassing from the surface waters to the atmosphere, while negative values indicate a CO_2 flux from the atmosphere to the ocean. The air-sea CO_2 flux in the Pacific was constantly positive throughout our study, fluctuating from 4.2 to 14.0 mmol C m^{-2} d^{-1} over time (Fig. 5a). The minima of FCO_2 occurred on day 26 and 30, while the maximum occurred on day 32 when near surface wind was the highest (2.89 m s^{-1}; Fig. 5b), corresponding to the minima and maxima of surface pCO_2. Co-occurring with a decrease in surface temperature to below 19℃ after day 36 (Fig 5c), FCO_2 slightly declined from ~10 to ~6 mmol C m^{-2} d^{-1} (Fig. 5a). FCO_2 was positively correlated with near surface wind speed (R^2 = 0.4). No correlation was found between FCO_2 and temperature (R^2 = 0).
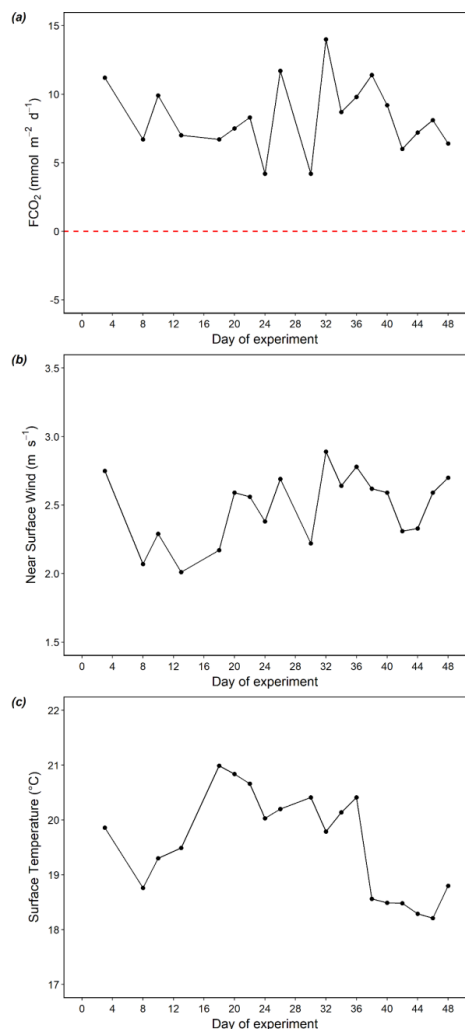
Figure 5 Temporal dynamics of surface air-sea CO₂ flux (a), near surface wind speed (b) and surface temperature (c) in the Pacific.
FCO₂ > 0 (above red dashed line) indicates CO₂ outgassing from the sea surface to the atmosphere. FCO₂ < 0 (below red dashed
line) indicates a CO₂ flux from the atmosphere to the sea.

4 Discussion

4.1 Quality control and propagated uncertainties

To compare the sensitivity of different calculated variables to uncertainties in the input variables, the propagated uncertainties

were averaged for each calculated variables, reported in numerical values and percentages relative to the calculated values of

each variable (Table 1). Among the 4 reported variables, Ω_{Ca} and Ω_{Ar} were the most sensitive to uncertainties in pH_T and TA

with an average uncertainty of 5.1%. This adds ambiguity to whether the bottom water (10-17 m for day 3-28; 12.5-17 m for

day 29-50) in the Pacific was undersaturated with respect to aragonite when Ω_{Ar} was oscillating near 1 (Fig. 4d). The

propagated uncertainty in pCO_2 was slightly lower (3.8%) while DIC was the least sensitive (0.3%).

We examined the internal consistency between DIC measurements and calculations. DIC was measured from day 3 until the

malfunction of the instrument on day 10. In total, 53 sets of measured DIC and calculated DIC (from measured pH_T and TA)

values were obtained from day 3 to day 10 and compared to test their consistency (Fig. 6a). The calculated DIC values were

334   generally in agreement with the measured values (R^2 = 0.985, p < 0.005), showing that the calculations made an overall good

335   prediction for the measured DIC values. The average of the residuals (calculated DIC– measured DIC) was -8.27 ± 6.9 μmol

336   kg^{-1}, indicating an underestimation of calculated DIC. This result is consistent with a previous observation of underestimated

337   calculated DIC (pH_T, TA) compared with measured DIC when applying the same set of constants (-6.6 ± 7.9 μmol kg^{-1};

338   Raimondi et al., 2019). The reasons for such underestimation have not been addressed in previous studies and remain unclear.

339   No significant relationships with input variables pH_T and TA (R^2 = 0.12 for both) and temperature (R^2 = 0.30) were found in

340   the DIC residuals (salinity remained the same from day 3 to day 10). The lack of correlation with pH_T and TA indicated that

341   the underestimation in calculated DIC was not a result from changes in pH_T and TA. Although dissociation constants are

342   known to be salinity- and temperature-dependent, the lack of correlation between DIC residuals and temperature may be

343   attributed to the relatively narrow ranges of temperature in the mesocosms (17.9-20.9℃ from day 3-10). The offsets were

344   typically larger at lower temperatures (e.g., samples from the Arctic, Chen et al. 2015).

345   To assess the quality of carbonate chemistry measurements in this study, the stability and performance of measurements were

346   evaluated. The standard deviation of triplicate pH_T measurements varied up to 0.003 with an average of 0.0012 throughout the

347   whole experiment (Fig. 6b). The average standard deviation was in agreement with reported analytical precisions of pH (0.003,

348   Orr et al. 2018; 0.002, Raimondi et al., 2019; Ma et al., 2019).

349   For TA, triplicate measurements of CRM distributed to before and after the sample measurements were carried out on each

350   measuring day to monitor the stability of the measurement process and the performance of the system. Based on the offsets, a

351   correction factor was applied to the measured values of samples on each sampling day to calibrate for instrument drift. As

352   shown in Fig. 6c, 90.5% of the measured TA values of CRM fell between warning limits (UWL and LWL) with one data point

353   falling outside the control limits (UCL and LCL), overall suggesting a relatively stable measurement system. The average

354   measured TA was 2209.9 μmol kg^{-1}, which was 17.69 μmol kg^{-1} lower than the certified concentration of the CRM (2227.59

355   μmol kg^{-1}), indicating a relatively poor accuracy (compared to the suggested bias of less than 2 μmol kg^{-1}; Dickson et al., 2003;

356   Dickson et al., 2007). The poor accuracy could be attributed to the fact that the concentration of the acid titrant was not checked

357   after being prepared, as suggested in the protocol (Dickson et al., 2003). A range control chart was computed based on duplicate

358   measurements of CRM made prior to the sample measurements on each sampling day to evaluate the consistency of the offset

359   between measured and certified TA values over the course of the study (Fig. 6d; Dickson et al., 2007). The absolute difference

360   (range) between the repeated CRM mesaurements was on average 1.4 μmol kg^{-1}. All the range values fell below the UWL

361   (3.50 μmol kg^{-1}; Fig. 6d), suggesting a relatively good precision of the measurement system.
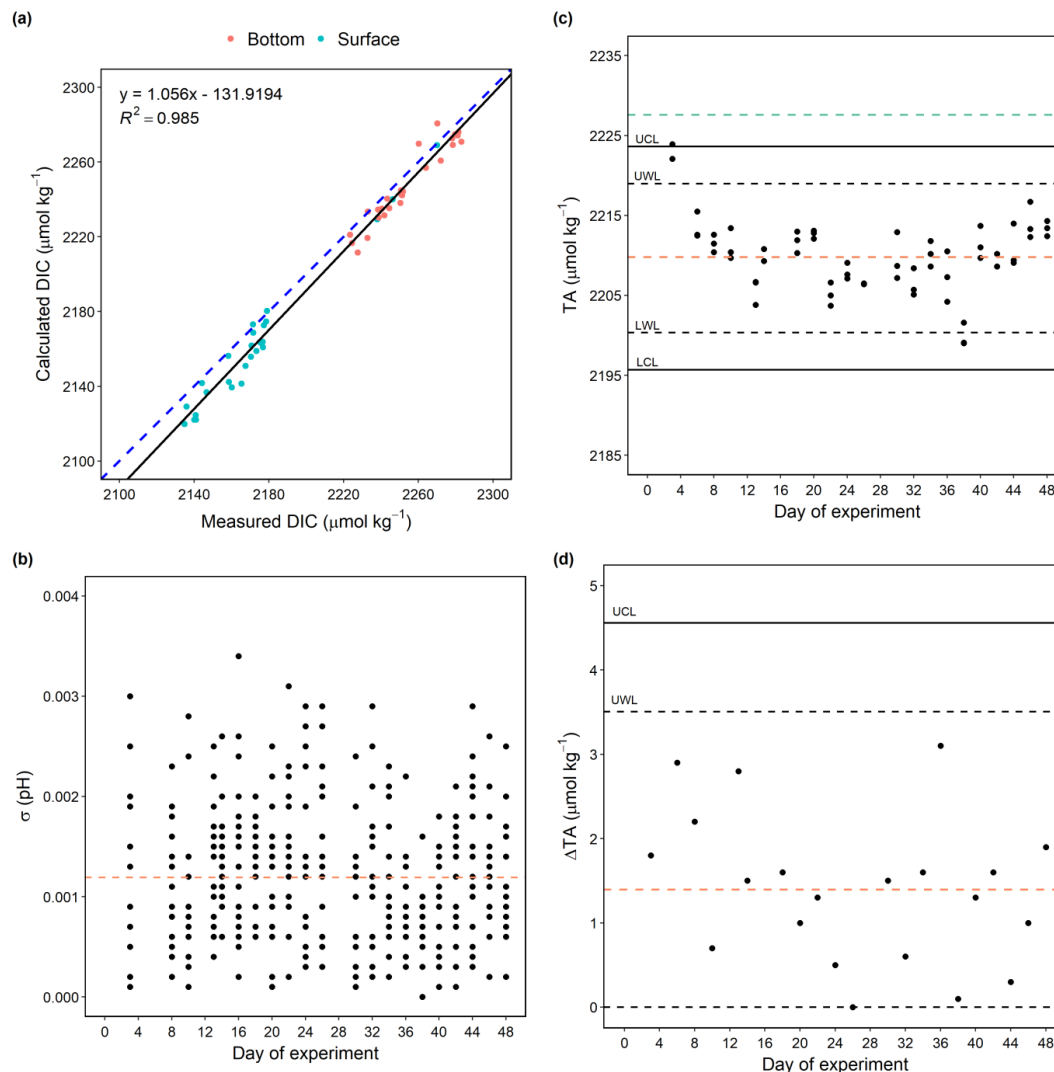
Figure 6 Comparison of calculated values of DIC (pH$_T$, TA) and measured values (a). The black line is the regression line, with the corresponding equation and R^2 shown in the top-left corner. The blue dashed line shows the regression line forced through the origin. Standard deviations of all the triplicate pH$_T$ measurements on each sampling day over the study period. Orange dashed line shows the average (n = 377) of the standard deviations (b). TA values of CRM measurements on each sampling day over the study period. Orange dashed line shows the average (n = 62) of the measured values and green dashed line indicates the certified value of the CRM (c). The absolute difference in TA values between duplicate CRM measurements (range) on each sampling day over the study period. Orange dashed line shows the average (n = 21) of the ranges (d). Abbreviation: UCL, upper control limit. UWL, upper warning limit. LWL, lower warning limit. LCL, lower control limit.

4.2 CO$_2$ responses to the simulated upwelling event

At the beginning of the experiment, surface pCO$_2$ levels in the mesocosms were >500 µatm (Fig. 3c). This suggests that we initially enclosed an upwelled water mass that was enriched with respiratory CO$_2$. The addition of OMZ water with high concentrations of CO$_2$ to the mesocosms reduced the surface pH$_T$ by 0.1-0.2 and increased the surface pCO$_2$ to >900 µatm (except for M7, which was 819.4 µatm on day 13). The simulated upwelling substantially reduced the variability in CO$_2$ between mesocosms because OMZ water addition replaced ~20 m^3 of seawater in each mesocosm (out of ~54 m^3). The enhanced pCO$_2$ level is comparable with our observations in the ambient Pacific water (>775 µatm; Fig. 3c). These values also

378   agree with reported observations for our study area in 2013 (>1,200 µatm in the upper 100 m and > 800 µatm at the surface;

379   Bates, 2018).

380   In the days after OMZ water addition, surface pCO_2 in the mesocosms dropped near or below the atmospheric level (405.22

381   µatm, NOAA/GML) with a decline in DIC by ~100 µmol kg^{-1} (except M3 and M4; Fig. 3c, d). The declining pCO_2 could be

382   partially attributed by CO_2 outgassing due to a high CO_2 gradient from the sea surface to the air. Due to a rare coastal El Nino

383   event (Garreaud, 2018), the CO_2 loss process may have been enhanced by a rapid surface warming (19.8-21.0 °C from day 14

384   to 36; Fig. 5) which reduced surface CO_2 solubility (Zeebe and Wolf-Gladrow, 2001). However, air-sea gas exchange could

385   not explain surface CO_2 under-saturation in relation to the atmosphere, as observed in response to OMZ water addition in some

386   mesocosms (Van Geen et al., 2000; Friederich et al., 2008; Fig. 3c). Biological production has typically one to four times

387   greater impacts on CO_2 drawdown than air-sea gas exchange in the equatorial Pacific where surface waters are exposed to

388   local wind stress (Feely et al., 2002). This interpretation is supported by the continuously high DIC in M4 where photosynthetic

389   biomass build-up was substantially lower (Fig. 3d). Hence, the depletion of nutrients (Fig. 2a, b) and increase in chl *a*

390   concentration (Fig 2c; Bach et al., 2020a) strongly suggest that the loss of DIC (except M4) was primarily driven by biological

391   uptake and phytoplankton growth. Nevertheless, it is difficult to dissect how much CO_2 was outgassed and how much was

392   taken up photosynthetically as we did not measure air-sea gas exchange in the mesocosms (please note that equations from

393   Wanninkhof, (2014) are not applicable for mesocosms).

394   Before OMZ water addition, dissolved inorganic N:P ratios in the mesocosms ranged from 1.6 to 3.5 (data not shown),

395   indicating N is the limiting nutrient in the water column (Bach et al., 2020a). Not surprisingly, the uptake of DIC was higher

396   in the "Low DIN" mesocosms which received more input of DIN from OMZ water addition, with on average 41.0 µmol kg^{-1}

397   higher drawdown compared to the "Very Low DIN" from day 13 to day 24 (excluding M3 and M4; Mann-Whitney U-Test, p

398   = 0.05; Table S1). This observation agrees with the general expectations that addition of limiting nutrients to water column

399   should enhance biological biomass build-up. Such differences in DIC uptake, however, were not reflected in the build-up of

400   particulate organic carbon (POC) in the mesocosms (excluding M3 and M4; Mann-Whitney U-Test, $p > 0.1$). As mentioned

401   above, the differences in OMZ-water DIN between the two treatments were minor and hence, their potential to trigger treatment

402   difference were small. Due to the developing N-limitation after the biomass build-up there much of the consumed DIC could

403   have been channelled to dissolved organic carbon (DOC) pool. Indeed, we observed a pronounced increase in DOC following

404   OMZ water addition (except for M4; Igarza et al., in prep, 2021). The increase in DOC may be attributed to extracellular

405   release by phytoplankton due to nutrient limitation, or cellular lysis of phytoplankton cells by bacteria (Myklestad 2000; Igarza

406   et al., in prep, 2021).

407   After day 24, variability in carbonate chemistry between individual mesocosms increased, with a general trend of recovering

408   from CO_2-undersaturated conditions during the peak of the bloom (except for M3 and M4; Fig. 3c). One factor that may have

409   controlled the differences in CO_2 increase are the mesocosm-specific phytoplankton succession patterns. A shift from a diatom-

410   dominated community to a dominance of dinoflagellates (in particular *Akashiwo sanguinea*) occurred when DIN was

411   exhausted, which was absent in M3 and M4 (Bach et al., 2020a). The different succession patterns in the plankton community

412   are the most likely explanation why M3 and M4 behaved differently from the others in terms of surface layer productivity, and

413   hence carbonate chemistry. Although the rate of DIN depletion in M3 and M4 were similar to the others, the reduction in pCO_2

414   in M3 experienced a 1-week delay which is consistent with the delayed build-up of chl *a* biomass (Fig. 2c, 3c). On the other

415   hand, the pCO_2 level in M4 remained constantly elevated throughout the experiment, as of a lack of a phytoplankton bloom

416   (Fig. 2c, 3c). M4 was the only mesocosm where a *A. sanguinea* remained undetectable, whereas a delayed and reduced

417   contribution by *A. sanguinea* was observed in M3. This strongly suggests that *A. sanguinea* was a key factor driving the trend

418   of carbonate chemistry in the mesocosms.

419 Near the end of the experiment, a slight decline in pCO_2 became apparent in the mesocosms which co-occurred with a second

420 phytoplankton bloom observed in the uppermost layer of the water column (Fig. 2c, 3c). This bloom was likely fuelled by

421 surface eutrophication due to defecating sea birds. During the last part of our experiment, Inca terns (*Larosterna inca*) were

422 frequently observed to rest on the roofs and the edges of the mesocosms (Bach et al., 2020a). Bird excrements, dropped into

423 the mesocosms, are known to be enriched in inorganic nutrients, especially ammonium (Bedard et al., 1980). The excrements

424 may also be high in dissolved organic nitrogen (DON), evidenced by a substantial increase in DON concentrations in the

425 mesocosm surface from day 38 onward (Igarza et al., in prep, 2021). The triggered surface eutrophication and phytoplankton

426 blooms were noticeable from an accumulation of chl a biomass above the mixed layer in the mesocosms near the end of the

427 study (Fig. 2c). As a result, another drawdown of DIC could be observed in the mesocosms except for M4, M6 and M8. While

428 the build-up of chl a was comparable with that triggered by OMZ water addition, the drawdown in DIC was less pronounced,

429 potentially counteracted by the release of CO_2 by enhanced respiration and remineralization following the previous bloom.

430 Also, the second bloom occurred in the top 2 meter in the mesocosms (Fig. 2c) where gas exchange can quickly replete the

431 DIC drawdown during photosynthesis and biomass build up.

4.3 Temporal changes of carbonate chemistry in the coastal Pacific near Callao

433 According to estimations by Takahashi et al. (2009) of global air-sea CO_2 fluxes, our study site in the equatorial Pacific (14°N-

434 14°S) is a major source of CO_2 to the atmosphere. Our near-coastal location showed high pCO_2 levels over the study period

435 (with an average of 1,078 μatm), with a sea-to-air CO_2 flux of 4.2-14.0 mmol C m^{-2} d^{-1} (Fig. 5). Compared to the criterion of

436 high CO_2 fluxes (5 mmol C m^{-2} d^{-1} or more) as proposed by Paulmier et al. (2008), our study site was a strong CO_2 source to

437 the atmosphere most of the time. These results of air-sea CO_2 fluxes were slightly higher than observations by Friederich et al.

438 (2008) along the coast of Peru in February, 2004-2006 (0.85-4.54 mol C m^{-2} yr^{-1}; spatially averaged for 5-15°S along the coast

439 of Peru). This is not surprising because Friederich et al. averaged the air-sea CO_2 fluxes for 0-200 km from shore where much

440 lower pCO_2 were observed offshore (< 600 μatm), compared to our nearshore study site. The decline in pCO_2 with increasing

441 distance from shore was driven by biological uptake and outgassing to the atmosphere (Friederich et al., 2008; Loucaides et

442 al., 2012). However, when compared to the magnitude of DIC drawdown triggered by upwelling events in the mesocosms, the

443 flux of CO_2 to the atmosphere was insignificant. Assuming a 10 m mixed layer in the Pacific with a DIC concentration of

444 2,200 μmol kg^{-1}, the DIC content below 1 m^2 surface area would be ~22 mol m^{-2}. With an upper bound outgassing of 14.2

445 mmol C m^{-2} d^{-1} over 10 days (day 13-24), the loss of CO_2 would only be 0.142 mol m^{-2}. On the other hand, the average DIC

446 drawdown of 118.2 μmol kg^{-1} in the "Very Low DIN" and 160.3 μmol kg^{-1} in the "Low DIN" mesocosms (M3 and M4

447 excluded) during this period accounts for 1.18 mol m^{-2} and 1.60 mol m^{-2}, respectively, over the same water column. This shows

448 that biological processes, drawing down CO_2, is stronger than loss by air-sea gas exchange.

449 During our study, we experienced a coastal El Niño event, which has been the strongest on record (compared to those recorded

450 in 1891 and 1925) and induced rapid sea surface warming of ~1.5°C and enhanced stratification (Garreaud, 2018). Previous

451 investigations showed that the impact of reduced upwelling on CO_2 fluxes is pronounced for upwelling areas (Feely et al.,

452 1999; Feely et al., 2002). A decline in upwelling of CO_2-enriched OMZ water results in a decrease in sea-to-air CO_2 fluxes.

453 For example, during the 1991-94 El Niño year, a total reduction in CO_2 fluxes to the atmosphere was reported for the equatorial

454 Pacific. They were only 30-80% of that of a non-El-Niño year (Feely et al., 1999; Feely et al., 2002). This is likely to be the

455 case for our study location. Most studies investigated air-sea CO_2 fluxes at larger time and regional scales (Feely et al., 1999;

456 Friederich et al., 2008; Takahashi et al., 2009). Therefore, it is difficult to conclude the magnitude of the coastal El Niño

457 influence on the local CO_2 fluxes in our study by comparing our results with previous observations. Nevertheless, our

458 observations can serve as a first evidence of carbonate chemistry dynamics in the coastal Peruvian upwelling system during a

459 coastal El Niño event. Observations of sea surface carbonate chemistry with a high temporal resolution (every-2nd-day) in near-

460 shore waters are scarce, as rarely covered by typical research expeditions in the open ocean (Takahashi et al., 2009; Franco et

461 al., 2014), especially during such an extremely rare coastal El Niño event. Comparisons of our data with previous or future

462 observations may enhance our understanding of how inorganic carbon cycling interact with extreme climate events in

463 upwelling systems.

464 CO_2-enriched OMZ water has been occasionally reported to be under-saturated with respect to aragonite (Feely et al., 2008;

465 Fassbender et al., 2011). In our study, calcite under-saturation did not occur in the mesocosms or in the Pacific (Fig. 4).

466 Aragonite under-saturation, however, was observed below the surface (10-17 m for day 3-28; 12.5-17 m for day 29-50) of the

467 Pacific at the start of the experiment (Fig. 4d), when pCO_2 was the highest (pCO_2 > 1100 µatm; Fig. 3c). Aragonite under-

468 saturation was also observed in the two deep water masses collected at deeper depths (30 m and 70 m) in the Pacific (Table

469 4). Throughout the study period, the aragonite saturation state fluctuated close to around 1 below the surface (Fig. 4d).

470 Considering the water column we sampled in the Pacific still belonged to the upper surface ocean, we could expect deeper and

471 more CO_2-enriched water in the underlying OMZ to be most likely under-saturated with respect to calcite and aragonite. Hence,

472 our observations of aragonite under-saturation in the Pacific suggest a potential risk of dissolution for marine calcifiers in

473 response to the on-going intensification and expansion of acidified OMZ water (Comeau et al., 2009; Lischka et al., 2011;

474 Maas et al., 2012).

475 **5 Conclusion**

476 Our observations in the mesocosms revealed that, following the addition of two OMZ water masses with different nutrient

477 signatures, there was a higher drawdown of DIC in response to slightly more DIN input from the OMZ water addition but no

478 difference in the build-up of POC and chl *a* (Fig. 2a, 2c, 3d). The timing of the first phytoplankton bloom was consistent with

479 a shift from a diatom-dominated community to *A. sanguinea* dominance in most mesocosms, indicating that *A. sanguinea* was

480 a key factor driving the changes in carbonate chemistry under N-limited conditions. A second phytoplankton bloom was

481 triggered by defecations of Inca terns, which eased the N limitation in the mesocosms (Fig. 2c). These findings provide

482 improved insights into the links between upwelling-induced N limitation, phytoplankton community shifts and carbonate

483 chemistry dynamics in the Peruvian upwelling system.

484 The surrounding Pacific waters at the study site were characterized by constantly high pCO_2 levels (with an average of 1,078.1

485 µatm). Most CO_2 flux estimates have been conducted in the open ocean and few studies surveyed coastal regions (Takahashi

486 et al., 2009; Franco et al., 2014). Our study site was a strong CO_2 source to the atmosphere most of the time (4.2-14.2 mmol

487 C m^{-2} d^{-1}), despite a rare coastal El Niño event. However, evidence from our mesocosm experiment suggests biological

488 responses that draw down DIC can quickly turn a CO_2 source into a sink in the upwelling system. The influence of the co-

489 occurring coastal El Niño event on the local CO_2 fluxes remains unclear. Nevertheless, future carbonate chemistry fluctuations

490 are expected to be enhanced by expanding and intensifying ocean deoxygenation, as well as reducing buffer factors (Schulz et

491 al., 2019). Hence, it is essential to improve our understanding of the mechanisms driving the inorganic carbon cycling in

492 upwelling systems. As a unique dataset that characterized near-shore carbonate chemistry with a high temporal resolution

493 during a rare coastal El Niño event, our study gives important insights into the carbonate chemistry responses to extreme

494 climate events in the Peruvian upwelling system.

495 **Data availability**

496 All data will be made available on the permanent repository www.pangaea.de after publication.

Biogeosciences Open Access
Discussions
EGU

References

517 Albert, A., Echevin, V., Lévy, M. and Aumont, O.: Impact of nearshore wind stress curl on coastal circulation and primary
518 productivity in the Peru upwelling system, J. Geophys. Res. Oceans, 115(C12), https://doi.org/10.1029/2010JC006569, 2010.
519 Bach, L.T., Boxhammer, T., Larsen, A., Hildebrandt, N., Schulz, K.G. and Riebesell, U.: Influence of plankton community
520 structure on the sinking velocity of marine aggregates, Global Biogeochem. Cycles, 30(8), 1145-1165, 2016.
521 Bach, L. T., Paul, A. J., Boxhammer, T., von der Esch, E., Graco, M., Schulz, K. G., Achterberg, E., Aguayo, P., Arístegui, J.,
522 Ayón, P., Baños, I., Bernales, A., Boegeholz, A. S., Chavez, F., Chavez, G., Chen, S.-M., Doering, K., Filella, A., Fischer, M.,
523 Grasse, P., Haunost, M., Hennke, J., Hernández-Hernández, N., Hopwood, M., Igarza, M., Kalter, V., Kittu, L., Kohnert, P.,
524 Ledesma, J., Lieberum, C., Lischka, S., Löscher, C., Ludwig, A., Mendoza, U., Meyer, J., Meyer, J., Minutolo, F., Ortiz Cortes,
525 J., Piiparinen, J., Sforna, C., Spilling, K., Sanchez, S., Spisla, C., Sswat, M., Zavala Moreira, M., and Riebesell, U.: Factors
526 controlling plankton community production, export flux, and particulate matter stoichiometry in the coastal upwelling system
527 off Peru, Biogeosciences, 17, 4831–4852, https://doi.org/10.5194/bg-17-4831-2020, 2020a.
528 Bach, L. T., Paul, A., Boxhammer, T., von der Esch, E., Graco, M., Schulz, K. G., Achterberg, E. P., Aguayo, P., Arístegui,
529 J., Ayón, P., Banos, I., Bernales, A., Boegeholz, A. S., Chavez, F. P., Chen, S.-M., Doering, K., Filella, A., Fischer, M. A.,
530 Grasse, P., Haunost, M., Hennke, J., Hernandez-Hernandez, N., Hopwood, M., Igarza, M., Kalter, V., Kittu, L., Kohnert, P.,
531 Ledesma, J., Lieberum, C., Lischka, S., Löscher, C., Ludwig, A., Mendoza, U., Meyer, J., Meyer, J., Minutolo, F., Ortiz Cortes,
532 J., Piiparinen, J., Sforna, C., Spilling, K., Sanchez, S., Spisla, C., Sswat, M., Zavala Moreira, M., and Riebesell, U.: KOSMOS
533 2017 Peru mesocosm study: overview data, PANGAEA, https://doi.org/10.1594/PANGAEA.923395, 2020b.

534 Bakun, A. and Weeks, S.J.: The marine ecosystem off Peru: What are the secrets of its fishery productivity and what might its

535 future hold?, Prog. Oceanogr., 79(2-4), 290-299, https://doi.org/10.1016/j.pocean.2008.10.027, 2008.

536 Bates, N.R.: Seawater carbonate chemistry distributions across the Eastern South Pacific Ocean sampled as part of the

537 GEOTRACES project and changes in marine carbonate chemistry over the past 20 years, Front Mar. Sci., 5(398), 1-18,

538 https://doi.org/10.3389/fmars.2018.00398, 2018.

539 Beaudoing, H. and M. Rodell, NASA/GSFC/HSL: GLDAS Noah Land Surface Model L4 3 hourly 0.25 x 0.25 degree V2.1,

540 Greenbelt, Maryland, USA, Goddard Earth Sciences Data and Information Services Center (GES DISC), Accessed: [2021-04-

541 08], 10.5067/E7TYRXPJKWOQ, 2020

542 Bedard, J., Therriault, J.C. and Berube, J.: Assessment of the importance of nutrient recycling by seabirds in the St. Lawrence

543 Estuary, Can. J. Fish. Aquat. Sci. *37*(4), 583-588, https://doi.org/10.1139/f80-074, 1980.

544 Bockmon, E.E. and Dickson, A.G.: A seawater filtration method suitable for total dissolved inorganic carbon and pH analyses,

545 Limnol. Oceanogr. Methods, 12(4), 191-195, https://doi.org/10.4319/lom.2014.12.191, 2014.

546 Bopp, L., Resplandy, L., Orr, J.C., Doney, S.C., Dunne, J.P., Gehlen, M., Halloran, P., Heinze, C., Ilyina, T., Seferian, R. and

547 Tjiputra, J.: Multiple stressors of ocean ecosystems in the 21st century: projections with CMIP5 models, Biogeosciences, 10,

548 6225-6245, https://doi.org/10.5194/bg-10-6225-2013, 2013.

549 Capone, D.G. and Hutchins, D.A.: Microbial biogeochemistry of coastal upwelling regimes in a changing ocean, Nat. Geosci.,

550 6(9), 711, https://doi.org/10.1038/ngeo1916, 2013.

551 Carter, B.R., Radich, J.A., Doyle, H.L. and Dickson, A.G.: An automated system for spectrophotometric seawater pH

552 measurements, Limnol. Oceanogr. Methods, 11(1), 16-27, https://doi.org/10.4319/lom.2013.11.16, 2013.

553 Chavez, F.P. and Messié, M.: A comparison of eastern boundary upwelling ecosystems, Prog. Oceanogr., 83(1-4), 80-96,

554 https://doi.org/10.1016/j.pocean.2009.07.032, 2009.

555 Chavez, F.P., Bertrand, A., Guevara-Carrasco, R., Soler, P. and Csirke, J.: The northern Humboldt Current System: Brief

556 history,   present   status   and   a   view   towards   the   future,   Prog.   Oceanogr.,   79,   95-105,

557 https://doi.org/10.1016/j.pocean.2008.10.012, 2008.

558 Chen, B., Cai, W.J. and Chen, L.: The marine carbonate system of the Arctic Ocean: assessment of internal consistency and

559 sampling considerations, summer 2010, Mar. Chem., 176, 174-188, https://doi.org/10.1016/j.marchem.2015.09.007, 2015.

560 Clayton, T.D. and Byrne, R.H.: Spectrophotometric seawater pH measurements: total hydrogen ion concentration scale

561 calibration of m-cresol purple and at-sea results, Deep Sea Res. Part I Oceanogr. Res. Pap., 40(10), 2115-2129,

562 https://doi.org/10.1016/0967-0637(93)90048-8, 1993.

563 Comeau, S., Gorsky, G., Jeffree, R., Teyssié, J.L. and Gattuso, J.P.: Impact of ocean acidification on a key Arctic pelagic

564 mollusc (Limacina helicina). Biogeosciences, *6*(9), https://doi.org/10.5194/bg-6-1877-2009, 2009.

565 Cooperative Global Atmospheric Data Integration Project: Multi-laboratory compilation of atmospheric carbon dioxide data

566 for   the   period   1957-2018;   obspack_co2_1_GLOBALVIEWplus_v5.0_2019-08-12;   NOAA   Earth   System   Research

567 Laboratory, Global Monitoring Division. http://dx.doi.org/10.25925/20190812, 2019.

568 Correa, D., Tam, J., Pasapera, J., Saavedra, M. and Ingunza, A.: Modeling marine circulation and hypothetical discharges in

569 Callao Bay, Peru, Inf. Inst. Mar Peru, 35(3), 181-192, 2008.

570 Coverly, S., Kérouel, R. and Aminot, A.: A re-examination of matrix effects in the segmented-flow analysis of nutrients in sea

571 and estuarine water, Anal. Chim. Acta, 712, 94-100, 2012.

572 Cyronak, T., Schulz, K.G. and Jokiel, P.L.: The Omega myth: what really drives lower calcification rates in an acidifying

573 ocean, ICES J. Mar. Sci., 73(3), 558-562, https://doi.org/10.1093/icesjms/fsv075, 2016.

574 Czerny, J., Schulz, K.G., Krug, S.A., Ludwig, A. and Riebesell, U.: The determination of enclosed water volume in large

575 flexible-wall mesocosms "KOSMOS", Biogeosciences, 10(3), 1937-1941, https://doi.org/10.5194/bg-10-1937-2013, 2013.

576 Dale, A.W., Sommer, S., Lomnitz, U., Montes, I., Treude, T., Liebetrau, V., Gier, J., Hensen, C., Dengler, M., Stolpovsky, K.,

577 Bryant, L.D., and Wallmann, K.: Organic carbon production, mineralisation and preservation on the Peruvian margin,

578 Biogeosciences, 12, 1537-1559, https://doi.org/10.5194/bg-12-1537-2015, 2015.

579 Deutsch, C., Gruber, N., Key, R.M., Sarmiento, J.L. and Ganachaud, A.: Denitrification and N_2 fixation in the Pacific Ocean,

580 Global Biogeochem. Cycles, 15(2), 483-506, https://doi.org/10.1029/2000GB001291, 2001.

581 Deutsch, C., Sarmiento, J.L., Sigman, D.M., Gruber, N. and Dunne, J.P.: Spatial coupling of nitrogen inputs and losses in the

582 ocean, Nature, 445(7124), 163-167, https://doi.org/10.1038/nature05392, 2007.

583 Dickson, A.G.: Standards for ocean measurements, Oceanogr., 23(3), 34–47, https://doi:10.5670/oceanog.2010.22, 2010.

584 Dickson, A.G., Wesolowski, D.J., Palmer, D.A. and Mesmer, R.E.: Dissociation constant of bisulfate ion in aqueous sodium

585 chloride solutions to 250. degree, C, J. Phys. Chem., 94(20), 7978-7985, https://doi.org/10.1021/j100383a042, 1990.

586 Dickson, A.G., Afghan, J.D. and Anderson, G.C.: Reference materials for oceanic CO_2 analysis: a method for the certification

587 of total alkalinity, Mar. Chem., 80(2-3), 185-197, https://doi.org/10.1016/S0304-4203(02)00133-0, 2003.

588 Dickson, A.G., Sabine, C.L. and Christian, J.R.: Guide to best practices for ocean CO2 measurements, North Pacific Marine

589 Science Organization, 2007.

590 Dlugokencky, E. and Tans, P.: NOAA/GML (www.esrl.noaa.gov/gmd/ccgg/trends/)

591 Doney, S.C., Ruckelshaus, M., Duffy, J.E., Barry, J.P., Chan, F., English, C.A., Galindo, H.M., Grebmeier, J.M., Hollowed,

592 A.B., Knowlton, N. and Polovina, J.: Climate change impacts on marine ecosystems, Ann. Rev. Mar. Sci., 4, 11-37,

593 https://doi.org/10.1146/annurev-marine-041911-111611, 2012.

594 Douglas, N.K. and Byrne, R.H.: Achieving accurate spectrophotometric pH measurements using unpurified meta-cresol purple

595 Mar. Chem., 190, pp.66-72, 2017.

596 Echevin, V., Aumont, O., Ledesma, J. and Flores, G.: The seasonal cycle of surface chlorophyll in the Peruvian upwelling

597 system: A modelling study, Prog. Oceanogr., 79(2-4), 167-176, https://doi.org/10.1016/j.pocean.2008.10.026, 2008.

598 Fassbender A.J., Sabine C.L., Feely R.A., Langdon C., Mordy C.W.: Inorganic carbon dynamics during northern California

599 coastal upwelling, Cont. Shelf Res., 31(11), 1180-1192, https://doi.org/10.1016/j.csr.2011.04.006, 2011.

600 Fassbender, A.J., Sabine, C.L. and Feifel, K.M.: Consideration of coastal carbonate chemistry in understanding biological

601 calcification, Geophys. Res. Lett., 43(9), 4467-4476, https://doi.org/10.1002/2016GL068860, 2016.

602 Feely, R.A., Wanninkhof, R., Takahashi, T. and Tans, P.: Influence of El Niño on the equatorial Pacific contribution to

603 atmospheric CO_2 accumulation, Nature, 398(6728), 597-601, https://doi.org/10.1038/19273, 1999.

604 Feely, R.A., Sabine, C.L., Hernandez-Ayon, J.M., Ianson, D. and Hales, B.: Evidence for upwelling of corrosive" acidified"

605 water onto the continental shelf, Science, 320(5882), 1490-1492, https://doi.org/10.1126/science.1155676, 2008.

606 Franco, A.C., Hernández-Ayón, J.M., Beier, E., Garçon, V., Maske, H., Paulmier, A., Färber-Lorda, J., Castro, R. and Sosa-

607 Ávalos, R.: Air-sea CO2 fluxes above the stratified oxygen minimum zone in the coastal region off Mexico. J. Geophys. Res.

608 Oceans, 119(5), 2923-2937, 2014.

609 Franz, J., Krahmann, G., Lavik, G., Grasse, P., Dittmar, T. and Riebesell, U.: Dynamics and stoichiometry of nutrients and

610 phytoplankton in waters influenced by the oxygen minimum zone in the eastern tropical Pacific, Deep Sea Res. Part I

611 Oceanogr. Res. Pap., 62, 20-31, https://doi.org/10.1016/j.dsr.2011.12.004, 2012.

612 Friederich, G.E., Ledesma, J., Ulloa, O. and Chavez, F.P.: Air–sea carbon dioxide fluxes in the coastal southeastern tropical

613 Pacific, Prog. Oceanogr., 79(2-4), 156-166, https://doi.org/10.1016/j.pocean.2008.10.001, 2008.

614 Fuenzalida, R., Schneider, W., Garcés-Vargas, J., Bravo, L. and Lange, C.: Vertical and horizontal extension of the oxygen

615 minimum zone in the eastern South Pacific Ocean, Deep Sea Res. Part II Top. Stud. Oceanogr., 56(16), 992-1003,

616 https://doi.org/10.1016/j.dsr2.2008.11.001, 2009.

617   Gafar, N.A. and Schulz, K.G.: A three-dimensional niche comparison of Emiliania huxleyi and Gephyrocapsa oceanica:

618   Reconciling observations with projections, Biogeosciences, 15(11), 3541-3560, https://doi.org/10.5194/bg-15-3541-2018,

619   2018.

620   Galán, A., Molina, V., Thamdrup, B., Woebken, D., Lavik, G., Kuypers, M.M. and Ulloa, O.: Anammox bacteria and the

621   anaerobic oxidation of ammonium in the oxygen minimum zone off northern Chile, Deep Sea Res. Part II Top. Stud.

622   Oceanogr., 56(16), 1021-1031, https://doi.org/10.1016/j.dsr2.2008.09.016, 2009.

623   Garreaud, R.D.: A plausible atmospheric trigger for the 2017 coastal El Niño. Int. J. Climatol., 38, e1296-e1302,

624   https://doi.org/10.1002/joc.5426, 2018.

625   Gattuso, J.P., Epitalon, J.M., Lavigne, H., Orr, J., Gentili, B., Hagens, M., Hofmann, A., Mueller, J.D., Proye, A., Rae, J. and

626   Soetaert, K.: Package 'seacarb', http://CRAN.R-project.org/package=seacarb, Accessed 5 Jun 2020, 2020.

627   Gilly, W.F., Beman, J.M., Litvin, S.Y. and Robison, B.H.: Oceanographic and biological effects of shoaling of the oxygen

628   minimum zone, Ann. Rev. Mar. Sci., 5, 393-420, https://doi.org/10.1146/annurev-marine-120710-100849, 2013.

629   Gruber, N.: Warming up, turning sour, losing breath: ocean biogeochemistry under global change, Philos. Trans. A Math.

630   Phys. Eng. Sci., 369(1943), 1980-1996, https://doi.org/10.1098/rsta.2011.0003, 2011.

631   Hamersley, M.R., Lavik, G., Woebken, D., Rattray, J.E., Lam, P., Hopmans, E.C., Damsté, J.S.S., Krüger, S., Graco, M.,

632   Gutiérrez, D. and Kuypers, M.M.: Anaerobic ammonium oxidation in the Peruvian oxygen minimum zone, Limnol. Oceanogr.,

633   52(3), 923-933, https://doi.org/10.4319/lo.2007.52.3.0923, 2007.

634   Haugan, P.M. and Drange, H.: Effects of CO_2 on the ocean environment, Energy Convers. Manag., *37*(6-8), 1019-1022,

635   https://doi.org/10.1016/0196-8904(95)00292-8, 1996.

636   Hauri, C., Gruber, N., Plattner, G.K., Alin, S., Feely, R.A., Hales, B. and Wheeler, P.A.: Ocean acidification in the California

637   current system, Oceanogr., 22(4), 60-71, 2009. www.jstor.org/stable/24861024. Accessed 22 June 2020.

638   Hauss, H., Franz, J.M. and Sommer, U.: Changes in N: P stoichiometry influence taxonomic composition and nutritional

639   quality of phytoplankton in the Peruvian upwelling, J. Sea Res., *73*, 74-85, https://doi.org/10.1016/j.seares.2012.06.010, 2012.

640   Hofmann, G.E., Barry, J.P., Edmunds, P.J., Gates, R.D., Hutchins, D.A., Klinger, T. and Sewell, M.A.: The effect of ocean

641   acidification on calcifying organisms in marine ecosystems: an organism-to-ecosystem perspective, Annu. Rev. Ecol. Evol.

642   Syst., 41, 127-147, https://doi.org/10.1146/annurev.ecolsys.110308.120227, 2010.

643   Igarza, M., Sánchez, S., Bernales, A., Gutiérrez, D., Meyer, J., Riebesell, U., Graco, M., Bach, L., Dittmar, T., and Niggemann,

644   J.: Dissolved organic matter production during an artificially-induced red tide off central Peru. Biogeosciences, in preparation,

645   2021.

646   Keeling, R.F., Körtzinger, A. and Gruber, N.: Ocean deoxygenation in a warming world, Ann. Rev. Mar. Sci., 2, 199-229,

647   https://doi.org/10.1146/annurev.marine.010908.163855, 2010.

648   Koeve, W. and Oschlies, A.: Potential impact of DOM accumulation of fCO2 and carbonate ion computations in ocean

649   acidification experiments, Biogeosciences (BG), 9, 3787-3798, https://doi.org/10.5194/bg-9-3787-2012, 2012.

650   Lam, P., Lavik, G., Jensen, M.M., van de Vossenberg, J., Schmid, M., Woebken, D., Gutiérrez, D., Amann, R., Jetten, M.S.

651   and Kuypers, M.M.: Revising the nitrogen cycle in the Peruvian oxygen minimum zone, Proc. Natl. Acad. Sci., 106(12), 4752-

652   4757, https://doi.org/10.1073/pnas.0812444106, 2009.

653   Lefèvre, N., Aiken, J., Rutllant, J., Daneri, G., Lavender, S. and Smyth, T.: Observations of pCO_2 in the coastal upwelling off

654   Chile: Spatial and temporal extrapolation using satellite data, J. Geophys. Res. Oceans, 107(C6), 8-1,

655   https://doi.org/10.1029/2000JC000395, 2002.

656   Levin, L.A. and Breitburg, D.L.: Linking coasts and seas to address ocean deoxygenation, Nat. Clim. Chang., 5(5), 401-403,

657   https://doi.org/10.1038/nclimate2595, 2015.

658   Lischka, S., Büdenbender, J., Boxhammer, T. and Riebesell, U.: Impact of ocean acidification and elevated temperatures on

659   early juveniles of the polar shelled pteropod Limacina helicina: mortality, shell degradation, and shell

660   growth, Biogeosciences, *8*, 919-932, http://dx.doi.org/10.5194/bg-8-919-2011, 2011.

661   Loucaides, S., Tyrrell, T., Achterberg, E.P., Torres, R., Nightingale, P.D., Kitidis, V., Serret, P., Woodward, M. and Robinson,

662   C.: Biological and physical forcing of carbonate chemistry in an upwelling filament off northwest Africa: Results from a

663   Lagrangian study, Global Biogeochem. Cycles, 26(3), https://doi.org/10.1029/2011GB004216, 2012.

664   Lueker, T.J., Dickson, A.G. and Keeling, C.D.: Ocean pCO_2 calculated from dissolved inorganic carbon, alkalinity, and

665   equations for K1 and K2: validation based on laboratory measurements of CO2 in gas and seawater at equilibrium, Mar. Chem.,

666   70(1-3), 105-119, https://doi.org/10.1016/S0304-4203(00)00022-0, 2000.

667   Ma, J., Shu, H., Yang, B., Byrne, R.H. and Yuan, D.: Spectrophotometric determination of pH and carbonate ion concentrations

668   in seawater: Choices, constraints and consequences, Anal. Chim. Acta, 1081, 18-31, https://doi.org/10.1016/j.aca.2019.06.024,

669   2019.Maas, A.E., Wishner, K.F. and Seibel, B.A.: The metabolic response of pteropods to acidification reflects natural CO_2-

670   exposure in oxygen minimum zones. Biogeosciences, *9*(2), 747-757, https://doi.org/10.5194/bg-9-747-2012, 2012.

671   Matear, R.J. and Hirst, A.C.: Long-term changes in dissolved oxygen concentrations in the ocean caused by protracted global

672   warming, Global Biogeochem. Cycles, 17(4), https://doi.org/10.1029/2002GB001997, 2003.

673   Matear, R.J., Hirst, A.C. and McNeil, B.I.: Changes in dissolved oxygen in the Southern Ocean with climate change, Geochem.

674   Geophys. Geosyst., 1(11), https://doi.org/10.1029/2000GC000086, 2000.

675   McNeil, C.L. and Merlivat, L.: The warm oceanic surface layer: Implications for CO2 fluxes and surface gas measurements,

676   Geophys. Res. Lett., 23(24), 3575-3578, https://doi.org/10.1029/96GL03426, 1996.

677   Mehrbach, C., Culberson, C.H., Hawley, J.E. and Pytkowicx, R.M.: Measurement of the apparent dissociation constants of

678   carbonic acid in seawater at atmospheric pressure 1, Limnol. Oceanogr., 18(6), 897-907,

679   https://doi.org/10.4319/lo.1973.18.6.0897, 1973.

680   Messié, M. and Chavez, F.P.: Nutrient supply, surface currents, and plankton dynamics predict zooplankton hotspots in coastal

681   upwelling systems. Geophys. Res. Lett., 44(17), 8979-8986, https://doi.org/10.1002/2017GL074322, 2017.

682   Mogollón, R. and Calil, P.H.: Modelling the mechanisms and drivers of the spatiotemporal variability of pCO_2 and air–sea

683   CO_2 fluxes in the Northern Humboldt Current System, Ocean Modelling, 132, 61-72,

684   https://doi.org/10.1016/j.ocemod.2018.10.005, 2018.

685   Montecino, V. and Lange, C.B.: The Humboldt Current System: Ecosystem components and processes, fisheries, and sediment

686   studies, Prog. Oceanogr., 83(1-4), 65-79, https://doi.org/10.1016/j.pocean.2009.07.041, 2009.

687   Morris, A.W. and Riley, J.P: The determination of nitrate in sea water, Anal. Chim. Acta, 29, 272-279,

688   https://doi.org/10.1016/S0003-2670(00)88614-6, 1963.

689   Mullin, J. and Riley, J.P.: The colorimetric determination of silicate with special reference to sea and natural waters, Anal.

690   Chim. Acta, 12, 162-176, https://doi.org/10.1016/S0003-2670(00)87825-3, 1955.

691   Murphy, J.A.M.E.S. and Riley, J.P: A modified single solution method for the determination of phosphate in natural waters,

692   Anal. Chim. Acta, 27, 31-36, https://doi.org/10.1016/S0003-2670(00)88444-5, 1962.

693   Myklestad, S.M.: Dissolved organic carbon from phytoplankton, In Mar. Chem., 111-148, Springer, Berlin, Heidelberg, 2000.

694   Orr, J.C., Epitalon, J.M. and Gattuso, J.P.: Comparison of ten packages that compute ocean carbonate chemistry, Biogeosci.

695   Discuss., 12(5), 1483-1510, https://doi.org/10.5194/bg-12-1483-2015, 2015.

696   Orr, J.C., Epitalon, J.M., Dickson, A.G. and Gattuso, J.P.: Routine uncertainty propagation for the marine carbon dioxide

697   system, Mar. Chem., 207, 84-107, https://doi.org/10.1016/j.marchem.2018.10.006, 2018.

698   Oschlies, A., Brandt, P., Stramma, L. and Schmidtko, S.: Drivers and mechanisms of ocean deoxygenation, Nat. Geosci., 11,

699   467–473, https://doi.org/10.1038/s41561-018-0152-2, 2018.

700 Paulmier, A., Ruiz-Pino, D. and Garçon, V.: The oxygen minimum zone (OMZ) off Chile as intense source of CO_2 and N_2O,

701 Cont. Shelf Res., 28(20), 2746-2756, https://doi.org/10.1016/j.csr.2008.09.012, 2008.

702 Paulmier, A., Ruiz-Pino, D. and Garçon, V.: CO_2 maximum in the oxygen minimum zone (OMZ), Biogeosciences, 8, 239-

703 252, https://doi.org/10.5194/bg-8-239-2011, 2011.

704 Pierrot, D., Lewis, E. and Wallace, D.W.R.: MS Excel program developed for CO2 system calculations, ORNL/CDIAC-105a,

705 Carbon Dioxide Information Analysis Center, Oak Ridge National Laboratory, US Department of Energy, Oak Ridge,

706 Tennessee, 2006.

707 Raimondi, L., Matthews, J.B.R., Atamanchuk, D., Azetsu-Scott, K. and Wallace, D.W.: The internal consistency of the marine

708 carbon dioxide system for high latitude shipboard and in situ monitoring, Mar. Chem., 213, 49-70,

709 https://doi.org/10.1016/j.marchem.2019.03.001, 2019.

710 Redfield, A.C.: The influence of organisms on the composition of seawater, The Sea, 2, 26-77, 1963.

711 Riebesell, U., Czerny, J., Bröckel, K.V., Boxhammer, T., Büdenbender, J., Deckelnick, M., Fischer, M., Hoffmann, D., Krug,

712 S.A., Lentz, U. and Ludwig, A.: A mobile sea-going mesocosm system–new opportunities for ocean change research,

713 Biogeosciences, 10(3), 1835-1847, https://doi.org/10.5194/bg-10-1835-2013, 2013.

714 Rodell, M., P.R. Houser, U. Jambor, J. Gottschalck, K. Mitchell, C. Meng, K. Arsenault, B. Cosgrove, J. Radakovich, M.

715 Bosilovich, J.K. Entin, J.P. Walker, D. Lohmann, and D. Toll: The Global Land Data Assimilation System, Bull. Amer.

716 Meteor. Soc., 85, 381-394, doi:10.1175/BAMS-85-3-381, 2004

717 RStudio Team (2015). RStudio: Integrated Development for R. RStudio, Inc., Boston, MA URL http://www.rstudio.com/.

718 Schmidtko, S., Stramma, L. and Visbeck, M.: Decline in global oceanic oxygen content during the past five decades, Nature,

719 542(7641), 335-339, 2017.

720 Schulz, K.G. and Riebesell, U.: Diurnal changes in seawater carbonate chemistry speciation at increasing atmospheric carbon

721 dioxide, Mar. Biol., 160(8), 1889-1899, https://doi.org/10.1007/s00227-012-1965-y, 2013.

722 Schulz, K.G., Bellerby, R.G.J., Brussaard, C.P.D., Büdenbender, J., Czerny, J., Engel, A., Fischer, M., Koch-Klavsen, S.,

723 Krug, S., Lischka, S. and Ludwig, A.: Temporal biomass dynamics of an Arctic plankton bloom in response to increasing

724 levels of atmospheric carbon dioxide, Biogeosciences, 10, 161-180, https://doi.org/10.5194/bg-10-161-2013, 2013.

725 Schulz, K.G., Bach, L.T., Bellerby, R.G., Bermúdez, R., Büdenbender, J., Boxhammer, T., Czerny, J., Engel, A., Ludwig, A.,

726 Meyerhöfer, M. and Larsen, A.: Phytoplankton blooms at increasing levels of atmospheric carbon dioxide: experimental

727 evidence for negative effects on prymnesiophytes and positive on small picoeukaryotes, Front. Mar. Sci., 4, 64,

728 https://doi.org/10.3389/fmars.2017.00064, 2017.

729 Schulz, K.G., Hartley, S. and Eyre, B.: Upwelling amplifies ocean acidification on the East Australian Shelf: implications for

730 marine ecosystems, Front. Mar. Sci., 6, 636, https://doi.org/10.3389/fmars.2019.00636, 2019.

731 Stramma, L., Johnson, G.C., Sprintall, J. and Mohrholz, V.: Expanding oxygen-minimum zones in the tropical oceans, Science,

732 320(5876), 655-658, https://doi.org/10.1126/science.1153847, 2008.

733 Stramma, L., Schmidtko, S., Levin, L.A. and Johnson, G.C.: Ocean oxygen minima expansions and their biological impacts,

734 Deep Sea Res. Part I Oceanogr. Res. Pap., 57(4), 587-595, https://doi.org/10.1016/j.dsr.2010.01.005, 2010.

735 Takahashi, T., Sutherland, S.C., Wanninkhof, R., Sweeney, C., Feely, R.A., Chipman, D.W., Hales, B., Friederich, G., Chavez,

736 F., Sabine, C. and Watson, A.: Climatological mean and decadal change in surface ocean pCO_2, and net sea–air CO_2 flux over

737 the global oceans, Deep Sea Res. Part II Top. Stud. Oceanogr., *56*(8-10), 554-577, https://doi.org/10.1016/j.dsr2.2008.12.009,

738 2009.

739 Taucher, J., Bach, L.T., Boxhammer, T., Nauendorf, A., Achterberg, E.P., Algueró-Muñiz, M., Arístegui, J., Czerny, J.,

740 Esposito, M., Guan, W. and Haunost, M.: Influence of ocean acidification and deep water upwelling on oligotrophic plankton

741 communities in the subtropical North Atlantic: insights from an in situ mesocosm study, Front Mar. Sci., 4, 85,

742 https://doi.org/10.3389/fmars.2017.00085, 2017.

743   Trenberth, K.E.: The definition of el nino, Bull. Am. Meteorol. Soc., 78(12), 2771-2778, https://doi.org/10.1175/1520-
744   0477(1997)078<2771:TDOENO>2.0.CO;2, 1997.

745   Uppström, L.R.: The boron/chlorinity ratio of deep-sea water from the Pacific Ocean, Deep Sea Res. and Oceanogr. Abstr.,
746   21, 161-162, https://doi.org/10.1016/0011-7471(74)90074-6, 1974.

747   Van Geen, A., Takesue, R.K., Goddard, J., Takahashi, T., Barth, J.A. and Smith, R.L.: Carbon and nutrient dynamics during
748   coastal upwelling off Cape Blanco, Oregon, Deep Sea Res. Part II Top. Stud. Oceanogr., 47(5-6), 975-1002,
749   https://doi.org/10.1016/S0967-0645(99)00133-2, 2000.

750   Volk, T. and Hoffert, M.I.: Ocean carbon pumps: Analysis of relative strengths and efficiencies in ocean-driven atmospheric
751   CO2 changes. The carbon cycle and atmospheric CO_2: natural variations Archean to present, 32, 99-110,
752   https://doi.org/10.1029/GM032p0099, 1985.

753   Wanninkhof, R.: Relationship between wind speed and gas exchange over the ocean revisited, Limnol. Oceanogr. Methods,
754   12(6), 351-362, https://doi.org/10.4319/lom.2014.12.351, 2014.

755   Weiss, R.: Carbon dioxide in water and seawater: the solubility of a non-ideal gas, Mar. Chem., 2(3), 203-215, 1974.

756   Whitney, F.A., Freeland, H.J. and Robert, M.: Persistently declining oxygen levels in the interior waters of the eastern subarctic
757   Pacific, Prog. Oceanogr., 75(2), 179-199, https://doi.org/10.1016/j.pocean.2007.08.007, 2007.

758   Zeebe, R.E. and Wolf-Gladrow, D.: CO_2 in seawater: equilibrium, kinetics, isotopes (No. 65), Gulf Professional Publishing,
759   2001.